

Dark matter in the Scotogenic model with spontaneous lepton number violation

Valentina De Romeri^a, Jacopo Nava^a, Miguel Puerta^a, Avelino Vicente^{a,b}

^(a) Instituto de Física Corpuscular, CSIC-Universitat de València, 46980 Paterna, Spain

^(b) Departament de Física Teòrica, Universitat de València, 46100 Burjassot, Spain

deromeri@ific.uv.es, jacopo.nava@ific.uv.es, miguel.puerta@ific.uv.es,
avelino.vicente@ific.uv.es

Abstract

Scotogenic models constitute an appealing solution to the generation of neutrino masses and to the dark matter mystery. In this work we consider a version of the Scotogenic model that breaks lepton number spontaneously. At this scope, we extend the particle content of the Scotogenic model with an additional singlet scalar which acquires a non-zero vacuum expectation value and breaks a global lepton number symmetry. As a consequence, a massless Goldstone boson, the majoron, appears in the particle spectrum. We discuss how the presence of the majoron modifies the phenomenology, both in flavor and dark matter observables. We focus on the fermionic dark matter candidate and analyze its relic abundance and prospects for both direct and indirect detection.

1 Introduction

The origin of neutrino masses and the nature of the dark matter (DM) component of the Universe are two of the most relevant open questions in current physics. Regarding the former, neutrino oscillation experiments have robustly established the existence of non-zero neutrino masses and lepton mixings. In fact, some of the oscillation parameters have been already determined with great accuracy [1]. Since the Standard Model (SM) of particle physics does not include a mechanism for the generation of neutrino masses, an extension is called for. Similarly, the Planck collaboration has determined that about 27% of the energy-matter content of the Universe is in the form of DM [2]. It is often assumed that the DM is made of particles, but no state in the SM spectrum has the required properties to play such a role. Again, this motivates the exploration of scenarios beyond the SM.

There are many neutrino mass models. Among them, radiative models (models that induce neutrino masses at the loop level) are particularly well motivated, since they naturally explain the smallness of neutrino masses due to the loop suppression. Pioneer work on radiative models can be found in [3–6], while for a recent review we refer to [7]. Furthermore, tree-level contributions to neutrino masses are often forbidden by a conserved \mathbb{Z}_2 symmetry which, in addition, stabilizes the lightest \mathbb{Z}_2 -odd state. Provided it has the correct quantum numbers and can be produced in the early Universe in the correct amount, this state is a valid DM candidate. Therefore, radiative models offer a good solution to simultaneously address the origin of neutrino masses and the DM problem. A prime example of such class of models is the Scotogenic model [8]. This model introduces an additional $SU(2)_L$ doublet, η , and three generations of fermion singlets, N , all charged under a \mathbb{Z}_2 parity. These ingredients suffice to generate neutrino masses at the 1-loop level and provide a viable DM candidate.

In most neutrino mass models, neutrinos are Majorana fermions. This is precisely the case of the Scotogenic model. In this class of models, $U(1)_L$ — where L stands for lepton number — is broken in two units. The breaking can be explicit, due to the presence of lepton number violating parameters in the Lagrangian, or spontaneous, if the minimum of the scalar potential of the model does not preserve the symmetry. In the *standard* Scotogenic model [8] the breaking is explicit. In contrast, in this paper we consider a version of the Scotogenic model that breaks lepton number spontaneously. This is achieved by extending the particle content of the model with an additional singlet scalar, denoted as σ , which acquires a non-zero vacuum expectation value (VEV) and breaks the global $U(1)_L$ symmetry. As a consequence, the spectrum of the theory contains a massless Goldstone boson, the majoron, J [9–13]. This state leads to novel phenomenological predictions, both in flavor observables (due to the existence of new channels such as $\ell_\alpha \rightarrow \ell_\beta J$) and in the DM sector (due to the existence of new processes in the early Universe).

Several works combining spontaneous lepton number breaking with the Scotogenic generation of fermion masses can be found in the literature. We highlight [14], which also studies the DM phenomenology of the Scotogenic model with spontaneous lepton number violation. We build upon this previous work and go beyond it in several ways. First of all, our analysis takes into account a wide variety of lepton flavor violating (LFV) constraints, including processes that involve the majoron either virtually or as a particle in the final state. We confirm the results of [14], but also discuss in further detail some aspects of the DM phenomenology of the model. A high-energy extension of the Scotogenic model featuring a massless majoron was also introduced in [15], while Ref. [16] proposes a model with spontaneous lepton number violation that induces a small 1-loop mass for a dark Majorana fermion *à la Scotogenic*. The authors of [17] studied electroweak baryogenesis in an extended Scotogenic scenario including a majoron, whereas the possible Scotogenic origin of the small lepton number violation of the inverse seesaw was discussed in [18]. Finally, the spontaneous breaking of a gauged version of lepton number in a Scotogenic scenario was considered in [19].

The rest of the manuscript is organized as follows. We present the model in Sec. 2, where we define its basic ingredients, discuss its scalar sector and the generation of Majorana neutrino masses and briefly comment on the possible DM candidates. The most important experimental bounds that constrain our scenario are discussed in Sec. 3, while the results of our numerical study are presented in Sec. 4. Finally, we summarize and draw our conclusions

in Sec. 5.

2 The model

We consider a variant of the original Scotogenic model. The SM particle content is extended by adding the $SU(2)_L$ scalar doublet η , the scalar singlet σ and three generations of fermion singlets N . The scalar doublets of the model can be decomposed into $SU(2)_L$ components as

$$H = \begin{pmatrix} H^+ \\ H^0 \end{pmatrix}, \quad \eta = \begin{pmatrix} \eta^+ \\ \eta^0 \end{pmatrix}. \quad (1)$$

Here H is the usual SM Higgs doublet. We impose the conservation of a global $U(1)_L$ symmetry which can be identified with lepton number. Finally, we also introduce the usual \mathbb{Z}_2 parity of the Scotogenic model, under which N and η are odd while the rest of the fields are even.¹ The particle content of the model and the representations under the gauge and global symmetries are summarized in Table 1.

The most general Yukawa Lagrangian, involving the new particles compatible with all symmetries, can be written as

$$\mathcal{L}_Y = y \bar{\ell}_L \eta N + \kappa \sigma \bar{N}^c N + \text{h.c.}, \quad (2)$$

where y and κ are 3×3 matrices. In the following, we take κ to be diagonal without loss of generality. The most general scalar potential is given by

$$\begin{aligned} \mathcal{V} = & m_H^2 H^\dagger H + m_\eta^2 \eta^\dagger \eta + m_\sigma^2 \sigma^* \sigma + \frac{\lambda_1}{2} (H^\dagger H)^2 + \frac{\lambda_2}{2} (\eta^\dagger \eta)^2 + \frac{\lambda_\sigma}{2} (\sigma^* \sigma)^2 \\ & + \lambda_3 (H^\dagger H) (\eta^\dagger \eta) + \lambda_3^{H\sigma} (H^\dagger H) (\sigma^* \sigma) + \lambda_3^{\eta\sigma} (\eta^\dagger \eta) (\sigma^* \sigma) \\ & + \lambda_4 (H^\dagger \eta) (\eta^\dagger H) + \left[\frac{\lambda_5}{2} (H^\dagger \eta)^2 + \text{h.c.} \right], \end{aligned} \quad (3)$$

where m_H^2 , m_η^2 and m_σ^2 are parameters with dimension of mass² and the rest of the parameters are dimensionless.

2.1 Symmetry breaking and scalar sector

We will assume that the scalar potential parameters are such that a minimum is found for the configuration

$$\langle H^0 \rangle = \frac{v}{\sqrt{2}}, \quad \langle \eta^0 \rangle = 0, \quad \langle \sigma \rangle = \frac{v_\sigma}{\sqrt{2}}. \quad (4)$$

Here $v \approx 246$ GeV is the usual electroweak VEV. This vacuum preserves the \mathbb{Z}_2 parity, which remains a conserved symmetry. In contrast, lepton number is spontaneously broken and a

¹Alternatively, one can assign $U(1)_L$ charges in such a way that the \mathbb{Z}_2 parity is obtained as a remnant symmetry after the spontaneous breaking of lepton number [15]. This is more economical in terms of symmetries, since the usual Scotogenic parity is not imposed, but automatically obtained from lepton number. However, the generation of the Scotogenic λ_5 coupling requires the introduction of a non-renormalizable operator.

	q_L	u_R	d_R	ℓ_L	e_R	N	H	η	σ
$SU(3)_C$	3	$\bar{3}$	$\bar{3}$	1	1	1	1	1	1
$SU(2)_L$	2	1	1	2	1	1	2	2	1
$U(1)_Y$	$\frac{1}{6}$	$\frac{2}{3}$	$-\frac{1}{3}$	$-\frac{1}{2}$	-1	0	$\frac{1}{2}$	$\frac{1}{2}$	0
$U(1)_L$	0	0	0	1	1	1	0	0	-2
\mathbb{Z}_2	$+$	$+$	$+$	$+$	$+$	$-$	$+$	$-$	$+$
GENERATIONS	3	3	3	3	3	3	1	1	1

Table 1: Particle content of the model and their representations under the gauge and global symmetries. q_L , ℓ_L , u_R , d_R , e_R and H are the usual SM fields.

Majorana mass term for the N singlets is induced, with

$$\frac{M_N}{2} = \kappa \frac{v_\sigma}{\sqrt{2}}. \quad (5)$$

The tadpole equations obtained by minimizing the scalar potential are given by

$$\frac{\partial \mathcal{V}}{\partial H^0} = \frac{v}{\sqrt{2}} \left(m_H^2 + \frac{\lambda_1 v^2}{2} + \frac{\lambda_3^{H\sigma} v_\sigma^2}{2} \right) = 0, \quad (6)$$

$$\frac{\partial \mathcal{V}}{\partial \sigma} = \frac{v_\sigma}{\sqrt{2}} \left(m_\sigma^2 + \frac{\lambda_\sigma v_\sigma^2}{2} + \frac{\lambda_3^{H\sigma} v^2}{2} \right) = 0. \quad (7)$$

Assuming the conservation of CP in the scalar sector, one can split the neutral scalar fields in terms of their real and imaginary components as

$$H^0 = \frac{1}{\sqrt{2}} (S_H + i P_H + v), \quad \eta^0 = \frac{1}{\sqrt{2}} (\eta_R + i \eta_I), \quad \sigma = \frac{1}{\sqrt{2}} (S_\sigma + i P_\sigma + v_\sigma). \quad (8)$$

The η_R and η_I fields do not mix with the rest of scalars due to the \mathbb{Z}_2 parity. In this case, the scalar potential contains the piece

$$\mathcal{V}_{\text{mass}}^N = \frac{1}{2} \text{Re}(z_i) (\mathcal{M}_R^2)_{ij} \text{Re}(z_j) + \frac{1}{2} \text{Im}(z_i) (\mathcal{M}_I^2)_{ij} \text{Im}(z_j), \quad (9)$$

where $z = \{H^0, \sigma\}$ and \mathcal{M}_R^2 and \mathcal{M}_I^2 are the 2×2 CP-even and CP-odd squared mass matrices, respectively. One finds

$$\mathcal{M}_R^2 = \begin{pmatrix} m_H^2 + \frac{3\lambda_1}{2} v^2 + \frac{\lambda_3^{H\sigma}}{2} v_\sigma^2 & \lambda_3^{H\sigma} v v_\sigma \\ \lambda_3^{H\sigma} v v_\sigma & m_\sigma^2 + \frac{3\lambda_\sigma}{2} v_\sigma^2 + \frac{\lambda_3^{H\sigma}}{2} v^2 \end{pmatrix}, \quad (10)$$

and

$$\mathcal{M}_I^2 = \begin{pmatrix} m_H^2 + \frac{\lambda_1}{2} v^2 + \frac{\lambda_3^{H\sigma}}{2} v_\sigma^2 & 0 \\ 0 & m_\sigma^2 + \frac{\lambda_\sigma}{2} v_\sigma^2 + \frac{\lambda_3^{H\sigma}}{2} v^2 \end{pmatrix}. \quad (11)$$

One can now use the tadpole equations in Eqs. (6)-(7) to evaluate these matrices at the minimum of the scalar potential. We obtain

$$\mathcal{M}_R^2 = \begin{pmatrix} \lambda_1 v^2 & \lambda_3^{H\sigma} v v_\sigma \\ \lambda_3^{H\sigma} v v_\sigma & \lambda_\sigma v_\sigma^2 \end{pmatrix}, \quad (12)$$

while the CP-odd mass matrix becomes identically zero as expected, since it has to provide two massless states: the unphysical Goldstone boson z that becomes the longitudinal component of the Z boson and a physical massless Goldstone boson associated to the spontaneous breaking of the lepton number, the majoron (J). Therefore, since σ is a gauge singlet field one can make the identification

$$J = P_\sigma, \quad z = P_H. \quad (13)$$

The CP-even states $\{S_H, S_\sigma\}$ mix leading to two massive states, h_1 and h_2 as follows:

$$\begin{pmatrix} h_1 \\ h_2 \end{pmatrix} = \mathcal{O} \begin{pmatrix} S_H \\ S_\sigma \end{pmatrix} = \begin{pmatrix} \cos \alpha & \sin \alpha \\ -\sin \alpha & \cos \alpha \end{pmatrix} \begin{pmatrix} S_H \\ S_\sigma \end{pmatrix}, \quad (14)$$

where \mathcal{O} is the 2×2 orthogonal matrix which diagonalizes the CP-even mass matrix, such that

$$\mathcal{O} \mathcal{M}_R^2 \mathcal{O}^T = \text{diag}(m_{h_1}^2, m_{h_2}^2), \quad (15)$$

and the mass eigenvalues are given by

$$m_{(h_1, h_2)}^2 = \frac{\lambda_1}{2} v^2 + \frac{\lambda_\sigma}{2} v_\sigma^2 \mp \sqrt{(2\lambda_3^{H\sigma} v v_\sigma)^2 + (\lambda_1 v^2 - \lambda_\sigma v_\sigma^2)^2}. \quad (16)$$

One of the two scalar masses has to be associated with the ~ 125 GeV SM Higgs boson and an additional CP-even state is present in the spectrum. The angle α is the doublet-singlet mixing angle and is given by

$$\tan \alpha = \frac{2\lambda_3^{H\sigma} v v_\sigma}{\lambda_1 v^2 - \lambda_\sigma v_\sigma^2 - \sqrt{(2\lambda_3^{H\sigma} v v_\sigma)^2 + (\lambda_1 v^2 - \lambda_\sigma v_\sigma^2)^2}}. \quad (17)$$

We focus now on the \mathbb{Z}_2 -odd scalars. The masses of the CP-even and CP-odd components of η^0 are given by

$$m_{(\eta_R, \eta_I)}^2 = m_\eta^2 + \frac{\lambda_3^{\eta\sigma}}{2} v_\sigma^2 + \frac{\lambda_3 + \lambda_4 \pm \lambda_5}{2} v^2, \quad (18)$$

thus as in the usual Scotogenic model the mass difference between η_R and η_I is controlled by the λ_5 coupling. Finally, the mass of the charged scalar fields η^\pm turns out to be

$$m_{\eta^\pm}^2 = m_\eta^2 + \frac{\lambda_3}{2} v^2 + \frac{\lambda_3^{\eta\sigma}}{2} v_\sigma^2. \quad (19)$$

2.2 Neutrino masses

Neutrino masses are induced at the 1-loop level, in the same way as in the standard Scotogenic model, as shown in Fig. 1. One finds the 3×3 neutrino mass matrix

$$(m_\nu)_{\alpha\beta} = \sum_{b=1}^3 \frac{y_{\alpha b} y_{\beta b}}{32\pi^2} m_{Nb} \left[\frac{m_{\eta_R}^2}{m_{Nb}^2 - m_{\eta_R}^2} \log \frac{m_{\eta_R}^2}{m_{Nb}^2} - \frac{m_{\eta_I}^2}{m_{Nb}^2 - m_{\eta_I}^2} \log \frac{m_{\eta_I}^2}{m_{Nb}^2} \right], \quad (20)$$

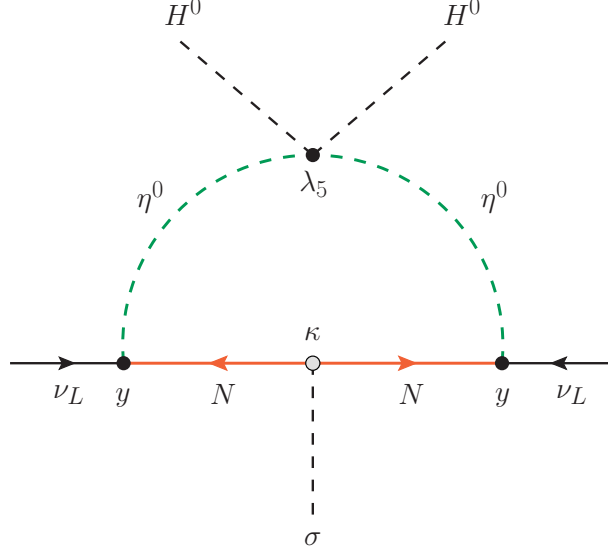


Figure 1: Generation of neutrino masses at the 1-loop level. In this diagram, η^0 denotes the real and imaginary components of the neutral component of the η doublet.

where m_{η_R} and m_{η_I} are the η_R and η_I masses, respectively, and $m_{N_b}^2$ are the diagonal elements of M_N . We note that neutrino masses vanish for $m_{\eta_R} = m_{\eta_I}$. This is consistent with the fact that $m_{\eta_R} - m_{\eta_I} \propto \lambda_5$, and in the limit $\lambda_5 \rightarrow 0$ a conserved lepton number can be defined. This allows one to assume $\lambda_5 \ll 1$ in a natural way [20].

2.3 Dark matter

The lightest \mathbb{Z}_2 -odd state is completely stable and can, in principle, be a good DM candidate. In this model, as in the standard Scotogenic model, this role can be played either by the lightest N state or by a neutral η field (η_R or η_I , depending on the sign of λ_5). In this work we will concentrate on the fermion DM and thus consider N_1 , the lightest singlet fermion, to be our DM candidate.

3 Constraints

Several experimental and theoretical constraints will be considered in our numerical analysis.

Boundedness from below

We demand the scalar potential to be bounded from below, which implies the following set of conditions [21]:

$$\lambda_1, \lambda_2, \lambda_\sigma \geq 0, \quad (21)$$

$$\lambda_3 \geq -\sqrt{\lambda_1 \lambda_2}, \quad (22)$$

$$\lambda_3^{H\sigma} \geq -\sqrt{\lambda_1 \lambda_\sigma}, \quad (23)$$

$$\lambda_3^{\eta\sigma} \geq -\sqrt{\lambda_2 \lambda_\sigma}, \quad (24)$$

$$\lambda_3 + \lambda_4 - |\lambda_5| \geq -\sqrt{\lambda_1 \lambda_2}. \quad (25)$$

Higgs boson production and decays

In our model, all Higgs boson production cross-sections at the LHC are suppressed with respect to the SM by c_α^2 , where $c_\alpha = \cos \alpha$ and α is the mixing angle in the CP-even scalar sector. In addition, Higgs decays are also affected in two ways. First, the rates of all visible Higgs decay channels are universally reduced due the abovementioned mixing. And second, new decay channels are available. The Higgs boson may decay invisibly to a pair of majorons or to a pair of DM particles, $h \rightarrow JJ$ and $h \rightarrow N_1 N_1$. The former will always be kinematically available, since the majoron is massless, whereas the latter requires $m_{N_1} \leq m_h/2$. The CMS collaboration has searched for invisible Higgs boson decays at the LHC [22], assuming a completely SM-like Higgs boson production through vector boson fusion. Therefore the limit derived in [22] translates into $c_\alpha^2 \text{BR}(h \rightarrow \text{invisible}) < 0.19$ at 95% C.L..

A proper phenomenological analysis must take into account both Higgs production and decays, including visible and invisible ones. In fact, the recent analysis [23] has clearly shown that the strongest constraints on the parameter space of our model are obtained by combining the bounds from visible and invisible Higgs decays. In particular, Figure 9 of this reference shows the limits obtained for our scenario. These are the constraints that will be considered in our numerical analysis.

Electroweak precision data

Bounds from electroweak precision data can also be used to constrain the parameter space of our model. In particular, the oblique parameters S , T and U [24] are known to capture the effect of heavy new fields affecting the gauge boson propagators. Their current determination is in good agreement with the SM expectations, although there is some room for new physics. In our analysis we considered the bounds [25]

$$S = -0.01 \pm 0.10, \quad (26)$$

$$T = 0.03 \pm 0.12, \quad (27)$$

$$U = 0.02 \pm 0.11. \quad (28)$$

Neutrino oscillation data

All the parameter points considered in our analysis comply with the constraints from neutrino oscillation experiments. This is guaranteed by means of a modified Casas-Ibarra parametrization [26], properly adapted to the Scotogenic model [27–29], which allows us to express the y Yukawa matrix as

$$y = \sqrt{\Lambda}^{-1} R \sqrt{\widehat{m}_\nu} U^\dagger. \quad (29)$$

Here Λ is a matrix defined as $\Lambda = \text{diag}(\Lambda_b)$, with

$$\Lambda_b = \frac{m_{Nb}}{32\pi^2} \left[\frac{m_{\eta_R}^2}{m_{Nb}^2 - m_{\eta_R}^2} \log \frac{m_{\eta_R}^2}{m_{Nb}^2} - \frac{m_{\eta_I}^2}{m_{Nb}^2 - m_{\eta_I}^2} \log \frac{m_{\eta_I}^2}{m_{Nb}^2} \right], \quad (30)$$

while R is an orthogonal matrix ($R^T R = R R^T = \mathbb{I}$), generally parametrized by three complex angles. Finally, U is the unitary matrix that brings m_ν to diagonal form as $U^T m_\nu U = \widehat{m}_\nu = \text{diag}(m_1, m_2, m_3)$, with m_i ($i = 1, 2, 3$) the neutrino physical masses. The entries of the unitary matrix U as well as the neutrino squared mass differences are measured in neutrino oscillation experiments. Our analysis will use the results of the global fit [1].

Majoron diagonal couplings to charged leptons

The interaction Lagrangian of majorons with charged leptons can be written as [30]

$$\mathcal{L}_{\ell\ell J} = J \bar{\ell}_\beta \left(S_L^{\beta\alpha} P_L + S_R^{\beta\alpha} P_R \right) \ell_\alpha + \text{h.c.}, \quad (31)$$

where $\ell_{\alpha,\beta}$ are the standard light charged leptons and $P_{L,R}$ are the usual chiral projectors. The $S_{L,R}$ couplings are induced at the 1-loop level in our model, as shown in [15]. The diagonal $S^{\beta\beta} = S_L^{\beta\beta} + S_R^{\beta\beta*}$ couplings are purely imaginary, due to the fact that majorons are pseudoscalar states, and are strongly constrained due to their potential impact on astrophysical observations. Large couplings to electrons or muons are excluded since they would lead to an abundant production of majorons in dense astrophysical media and an efficient cooling mechanism [31–35]. The authors of [33] used data from white dwarfs to set the bound

$$\text{Im } S^{ee} < 2.1 \times 10^{-13}, \quad (32)$$

while the supernova SN1987A was considered in [35] to establish the limit ²

$$\text{Im } S^{\mu\mu} < 2.1 \times 10^{-9}. \quad (33)$$

Finally, there are also laboratory bounds on the majoron diagonal couplings to charged leptons. In [30], the results of the OSQAR experiment [36], a light-shining-through-a-wall experiment, were used to find the approximate bounds $S^{ee} \lesssim 10^{-7}$ and $S^{\mu\mu} \lesssim 10^{-5}$. We note that these are clearly less stringent than the bounds obtained from astrophysical observations.

²Two alternative bounds are given in [35]. We decided to consider the most conservative one.

Lepton flavor violation

As in most neutrino mass models, LFV is a powerful constraint that strongly restricts the allowed parameter space of our model. Several processes will be considered in our analysis:

- The radiative decays $\ell_\alpha \rightarrow \ell_\beta \gamma$, which turn out to be the most constraining ones in most neutrino mass models. In particular, the MEG experiment restricts the $\mu \rightarrow e \gamma$ branching ratio to be smaller than 4.2×10^{-13} [37]. We also consider the analogous limits on τ LFV decays [25], but they are less stringent.
- The 3-body decays $\ell_\alpha \rightarrow \ell_\beta \ell_\gamma \ell_\gamma$, with $\beta = \gamma$ and $\beta \neq \gamma$. In this case we follow [38] and include the usual photon penguin contributions as well as other usually less relevant contributions, such as box diagrams. Majoron mediated contributions are also included, using the results derived in [30].
- The decays $\ell_\alpha \rightarrow \ell_\beta J$ with the majoron in the final state are also considered, as they constrain the off-diagonal $S_{L,R}$ couplings directly. For instance, the null results obtained in the search for the decay $\mu \rightarrow e J$ at TRIUMF [39] can be translated into the bound $|S^{e\mu}| < 5.3 \times 10^{-11}$ [40]. We use the analytical expressions for the majoron off-diagonal couplings to charged leptons in the Scotogenic model found in [15].
- $\mu - e$ conversion in nuclei, again following the analytical results in [38].

Majoron coupling to neutrinos

Constraints on the couplings of the majoron to neutrinos can be derived from astrophysics, since the majoron can have a significant impact on the explosion and cooling of supernovae (see e.g. [41]) and also from cosmic microwave background data [42]. Laboratory experiments searching for neutrinoless double beta decays (e.g. [43]) and possible effects on meson and lepton decays [44] also set limits on the magnitude of neutrino-majoron couplings. Among these, the most stringent ones are those derived from astrophysics, with constraints in the $\sim 10^{-7}$ ballpark. In our model, the interaction of majorons with neutrinos arises at the 1-loop level, similarly to the interaction with charged leptons, and the corresponding couplings are thus expected to be of the same order. Since the constraints on the couplings to charged leptons are orders of magnitude more stringent, we can safely ignore the constraints on the couplings to neutrinos in our analysis.

4 Numerical results

We now proceed to discuss the results of our analysis. To perform the numerical scan, we have first implemented the model in **SARAH** (version 4.11.0) [45], a **Mathematica** package for the analytical evaluation of all the information about the model.³ With this tool, we have created a source code for **SPheno** (version 4.0.2) [47, 48], thus allowing for an efficient numerical evaluation of all the analytical expressions derived with **SARAH**. We have also

³See [46] for a pedagogical introduction to the use of **SARAH**.

$\lambda_{2,3,4,\sigma} \in [10^{-6}, 1]$
$\lambda_5 \in [10^{-8}, 1]$
$m_{h_2} \in [20, 2000] \text{ GeV}$
$\kappa_{11} \in [0.01, 1]$
$m_\eta^2 \in [10^5, 10^7] \text{ GeV}^2 \text{ (or fixed)}$
$v_\sigma \in [0.5, 10] \text{ TeV}$

Table 2: Values of the main input parameters for the numerical scan.

computed several observables of interest in our model, including the lepton flavor violating ones, both analytically and with the help of `FlavorKit` [49], for an in-depth cross-check of their expressions. Finally, we have used `micrOmegas` (version 5.0.9) [50] to obtain the main DM observables, namely the DM relic density and direct and indirect detection predictions.

As already mentioned, while both the scalar $\eta_{R,I}$ and the fermions N_i are, in principle, viable DM candidates in this model, in our analysis we focus on the lightest Majorana fermion N_1 as the main component of the DM. We summarize our choice of parameters for the numerical scan in Tab. 2. Moreover, λ_1 is fixed by the condition of requiring $m_{h_1} = 125 \text{ GeV}$. In some numerical scans we have fixed the value of $m_{h_2} = 500 \text{ GeV}$ or the value of m_η^2 such that $m_{\eta_{R,I},\eta^\pm} - m_{N_1} \lesssim 20 \text{ GeV}$, as we will discuss in more detail below. With our choice of parameters, all the parameter points considered in our numerical scans easily pass the bounds from the S, T, U parameters. We note that with our choice of λ_4 and λ_5 values the mass splitting between the neutral and charged components of the η doublet is small (see Eqs. (18) and (19)). We have explicitly checked that only for $\lambda_4 \gtrsim 2$ the electroweak precision bounds become relevant, but we did not explore this region of parameter space in our scans. Since we want to focus on N_1 as the DM candidate, we further require that $m_{N_1} < m_{N_{2,3}}, m_{\eta_{R,I}}$. We have chosen normal hierarchy for the neutrino spectrum and considered the best-fit values for the neutrino oscillation parameters found by the global fit [1]. Finally, the three angles in the orthogonal R matrix are assumed to be real and taken randomly in our numerical scans.⁴

We first show in Fig. 2 the relic abundance of N_1 , as a function of its mass. For this specific scan, we have fixed $m_{h_2} = 500 \text{ GeV}$ to highlight the s -channel annihilation of N_1 via h_2 . In this figure, grey points denote solutions either leading to overabundant DM or excluded by any of the constraints listed in Sec. 3, or where the spin-independent N_1 -nucleon elastic scattering cross section is excluded by the most recent data from the LUX-ZEPLIN experiment [52]. Red points denote solutions which can reproduce the observed cold DM relic density, as they fall within the 3σ range obtained by the Planck satellite data [2], $\Omega_{N_1} h^2 = 0.120 \pm 0.0036$ (blue thin band). Solutions leading to underabundant DM (which would then require another DM candidate to explain the totality of the observed cold DM relic density) are depicted in blue. As can be seen from the plot, most of the solutions lead

⁴While more general scans with complex R matrices are in principle possible, we expect little impact on the DM phenomenology discussed here. Only in some specific regions of parameter space one may expect a change, due to the occurrence of very large Yukawa couplings at the prize of large cancellations [51], which we consider tuned.

to overabundant DM, except for points falling in the following regions: (i) a resonant region where $m_{N_1} \sim m_{h_1}/2 \sim 60$ GeV, (ii) a second resonant region where $m_{N_1} \sim m_{h_2}/2 \sim 250$ GeV and (iii) a region of coannihilations at higher m_{N_1} .

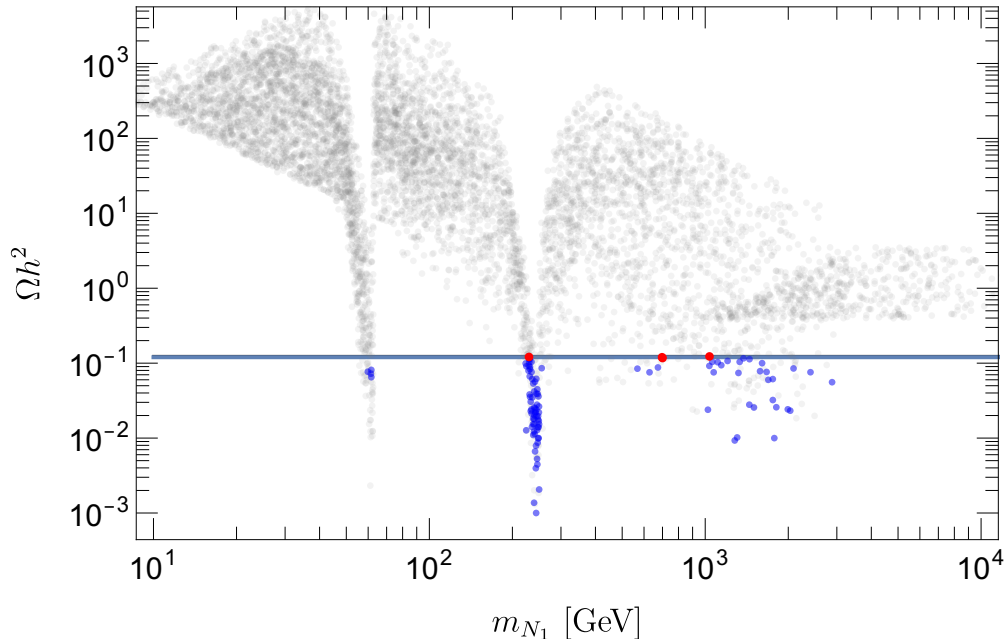


Figure 2: Relic abundance of N_1 as a function of m_{N_1} . Red points depict solutions in agreement with the cold DM measurement obtained from Planck data [2] (the blue thin band shows the 3σ interval) while blue points depict solutions leading to underabundant DM. Gray points are excluded by any of the constraints listed in Sec. 3 or due to an overabundant DM relic density.

To explore in more detail the third, high-mass region, we performed a second numerical scan in which we have varied the mass difference $\Delta = m_{\eta_R} - m_{N_1}$ in the $[0, 20]$ GeV range. In such a way, we have enforced N_1 to be in the $\sim [100 - 3000]$ GeV region, where coannihilations with $\eta_{R,I}$ and η^\pm are very relevant, thus reducing the relic abundance of N_1 . Figure 3 shows this region in parameter space, in which the DM relic density is set by coannihilations. The color code is the same as in Fig. 2. Compared to the result of the previous scan (Fig. 2), we can see that if coannihilations are relevant, more viable solutions can be found in the $m_{N_1} \sim [100, 3000]$ GeV region. We clarify that $\Delta < 20$ GeV is not motivated by any symmetry argument, but just a convenient parameter choice to focus our numerical analysis on a region in which coannihilations are more effective. Finally, we should also make a comment about the region with light η states ($m_{\eta_{R,I}}, m_{\eta^\pm} \lesssim 250$ GeV). These states can be pair-produced at the LHC via Drell-Yan processes. However, our choice of Δ implies a compressed spectrum with N , $\eta_{R,I}$ and η^\pm in a narrow window of just 20 GeV, thus implying soft leptons in the $\eta \rightarrow N\ell$ final decay. Searches for this type of signal exist, although not dedicated to our specific scenario. For instance, the ATLAS collaboration looked for direct slepton production with a compressed spectrum in [53]. This analysis assumes mass-degenerate 1st and 2nd generation sleptons decaying to flavor conserving final states,

whereas our scenario contains only a copy of the η doublet (and not two), with both flavor-conserving and flavor-violating decays. Therefore, the obtained limits are not applicable. Nevertheless, we note that some points with $\Delta \sim 10$ GeV, where the experimental searches are more efficient, must be excluded. A detailed analysis including this constraint is clearly beyond the scope of our work and would not have any impact on our conclusions.

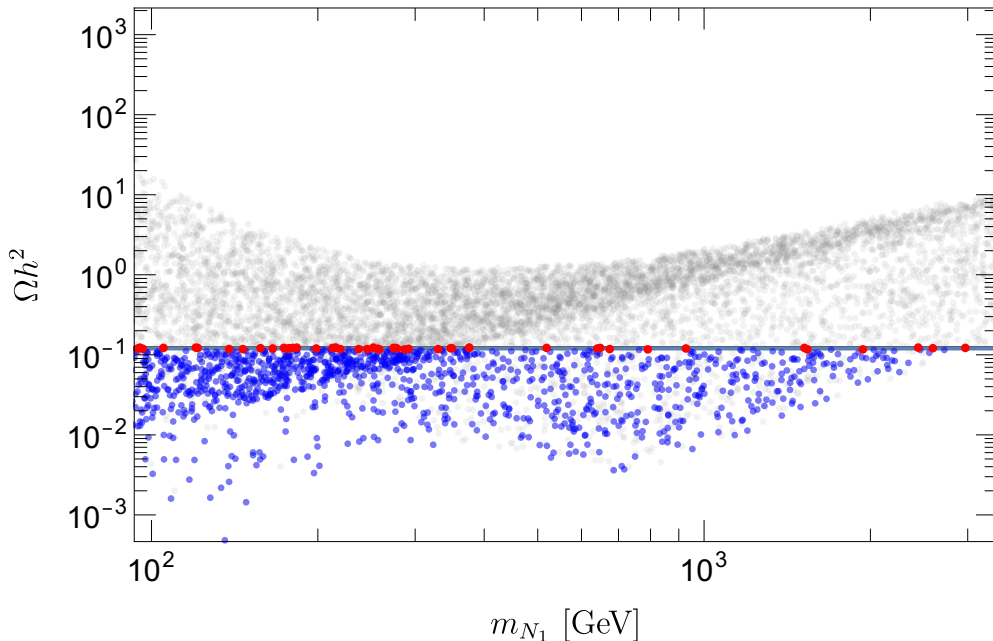


Figure 3: Relic abundance of N_1 as a function of m_{N_1} in the coannihilation region, where $\Delta \in [0, 20]$ GeV. Same color code as in Fig. 2.

Next we discuss the results for N_1 direct detection. In order to maximize the number of viable solutions, we focus again on the coannihilation region, and we show in Fig. 4 the spin-independent N_1 -nucleon elastic scattering cross section, σ_{SI} , as a function of the DM mass, m_{N_1} . The cross section shown in this figure is weighted by the relative abundance ξ , defined as

$$\xi = \frac{\Omega_{N_1}}{\Omega_{\text{DM,Planck}}} , \quad (34)$$

where $\Omega_{\text{DM,Planck}} h^2 = 0.120$ [2]. We apply the same color code as in Fig. 2, that is red points indicate solutions explaining the totality of observed DM, while blue points denote underabundant DM. The plain green line and dashed area indicate the current most stringent limit from the LUX-ZEPLIN experiment (LZ-2022) [52], while the black dashed line denotes the constraint from XENON1T (XENON1T-2018) [54]. Other (less stringent) constraints on σ_{SI} apply from the liquid xenon experiment PandaX-II [55] and from liquid argon experiments like DarkSide-50 [56] and DEAP-3600 [57], although they are not shown here. Future facilities including XENONnT [58], DarkSide-20k [59], ARGO [59] and DARWIN [60, 61] (see [62] for an overview) will be able to further inspect the parameter space of this model.

As for general reference, we further illustrate the expected discovery limit corresponding to the so-called “ ν -floor” from coherent elastic neutrino-nucleus scattering (CE ν NS) for a Ge target [63] (dashed orange line).⁵

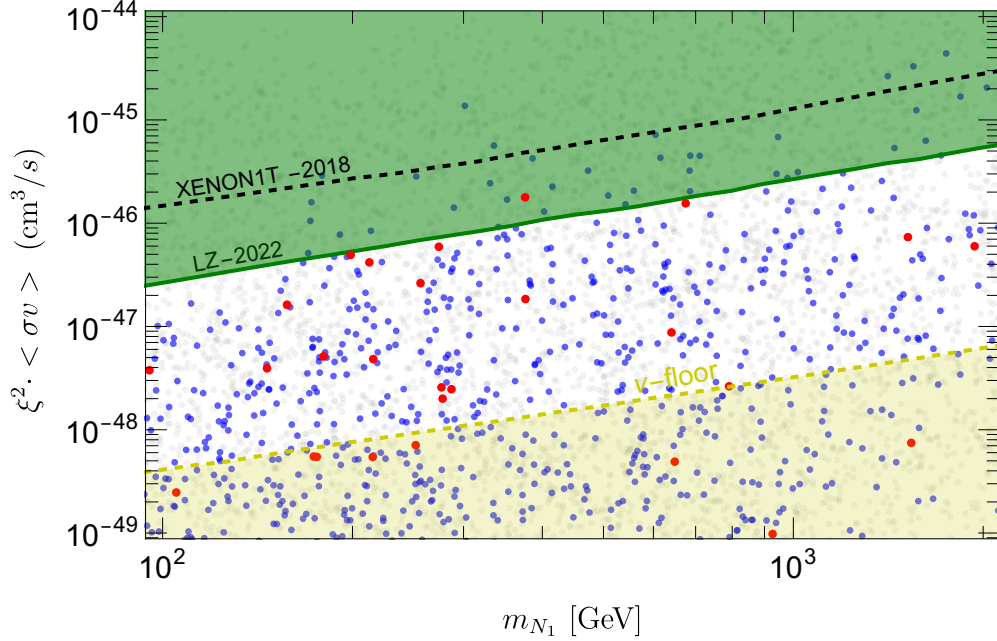


Figure 4: Spin-independent N_1 -nucleon elastic scattering cross section – weighted by the relative abundance – as a function of m_{N_1} . The green area is already excluded by the LUX-ZEPLIN experiment (LZ-2022) [52], while the black dashed line denotes the constraint from XENON1T (XENON1T-2018) [54]. The dashed orange curve indicates the expected discovery limit corresponding to the ν -floor from CE ν NS of solar and atmospheric neutrinos for a Ge target [63].

Finally, we have explored the predictions for the velocity-averaged cross section of N_1 annihilation into gamma rays. These are among the most suitable messengers to probe DM via indirect detection. We focus once more on the coannihilation region, i.e. on the high-mass range $m_{N_1} \sim 0.1\text{--}2$ TeV, where the annihilation channels $N_1 N_1 \rightarrow h_1 h_1, h_2 h_2, h_1 h_2, Z^0 Z^0, h_i J$ can be relevant. The hadronization of the final-state gauge bosons and Higgs bosons will produce neutral pions, which in turn can decay into photons thus giving rise to a gamma-ray flux with a continuum spectrum which may be within reach of DM indirect detection experiments. While a detailed calculation of the gamma-ray energy spectra produced by the annihilation of two N_1 particles in this specific model should be performed, in order to correctly compute exclusion bounds from existing gamma-ray data, this is out of the scope of this work. However, we can notice that the main annihilation channels in this high-mass range include Higgs bosons in the final state. The gamma-ray energy spectrum from DM $DM \rightarrow h_1 h_1$ annihilation channel is very similar to that from DM $DM \rightarrow W^+ W^-$ at $m_{N_1} \sim 1$

⁵Notice, however, that this should not be taken as a hard limit, as it can be overcome with different techniques and it has strong dependences on both the target material and a series of uncertainties (see for example [64–66] for more details).

TeV (see for instance Fig. 15 of [67]). In the following, for the sake of simplicity, we will compare our predictions with bounds obtained assuming W^+W^- as the main annihilation channel, to get an overall idea of how current data can constrain the parameter space of this model.

Charged cosmic rays can also be used to look for N_1 annihilations, even though their detection is more challenging due to uncertainties in the treatment of their propagation. For instance, AMS-02 data on the antiproton flux and the Boron to Carbon (B/C) ratio can be used to constrain the N_1 annihilation cross section [68–70]. With some caveats concerning the astrophysical uncertainties on the \bar{p} production, propagation and on solar modulation (see e.g. [71–73]), these bounds turn out to be stronger than gamma-ray limits from dwarf spheroidal satellite galaxies in some mass ranges. Following the same considerations as before, i.e. that the antiproton energy spectrum from $DM\ DM \rightarrow h_1 h_1$ annihilation channel is very similar to that from $DM\ DM \rightarrow W^+W^-$ at $m_{N_1} \sim 1$ TeV, we will compare our predictions to current limits on the N_1 annihilation cross section set by combination of \bar{p} and B/C data of AMS-02 [68, 69] assuming W^+W^- as the dominant annihilation channel. We show in Fig. 5 the N_1 total annihilation cross section — weighted by ξ^2 — versus its mass. The color code follow the same scheme as in Figs. 3, 4. We also depict the 95% C.L. upper limits currently set by the Fermi-LAT with gamma-ray observations of Milky Way dSphs (6 years, Pass 8 event-level analysis) [74] (red solid curve and shaded area) and from a combination of \bar{p} and B/C data of AMS-02 [68, 69] (green), both assuming $N_1 N_1 \rightarrow W^+W^-$ as main annihilation channel due to the considerations made before. We see that few solutions already fall within the region currently excluded by AMS-02 data. As already highlighted, while a dedicated analysis should be performed for this specific model, we can conclude that current \bar{p} and B/C data may be already excluding a relevant part of the parameter space. Forthcoming data will allow to further probe N_1 as a DM candidate via its multi-messenger signals.

As in many scenarios for neutrino mass generation, LFV processes strongly restrict the available parameter space of the model. In addition to $\mu \rightarrow e\gamma$, very commonly considered in phenomenological studies, our model also leads to signatures with the majoron in the final state, like $\mu \rightarrow eJ$. Figure 6 shows $BR(\mu \rightarrow eJ)$ as a function of $BR(\mu \rightarrow e\gamma)$. Again, we have focused on the coannihilation region. We first notice that some parameter points are already excluded by the current experimental limits on these LFV branching ratios. However, one can also see that our numerical scan also finds many valid parameter points leading to very low values of both $BR(\mu \rightarrow e\gamma)$ and $BR(\mu \rightarrow eJ)$, clearly below the discovery reach of planned experiments. This is not surprising, since we take random R matrices in our numerical scans, hence accidentally finding parameter points with suppressed $\mu - e$ flavor violation. While a slight correlation among these two observables can be observed in Fig. 6, $\mu \rightarrow e\gamma$ receives contributions from additional loop diagrams that do not involve the majoron. The two observables are hence independent. Interestingly, we find that $BR(\mu \rightarrow eJ)$ is generally more constraining than $BR(\mu \rightarrow e\gamma)$, although the difference is not very significant.

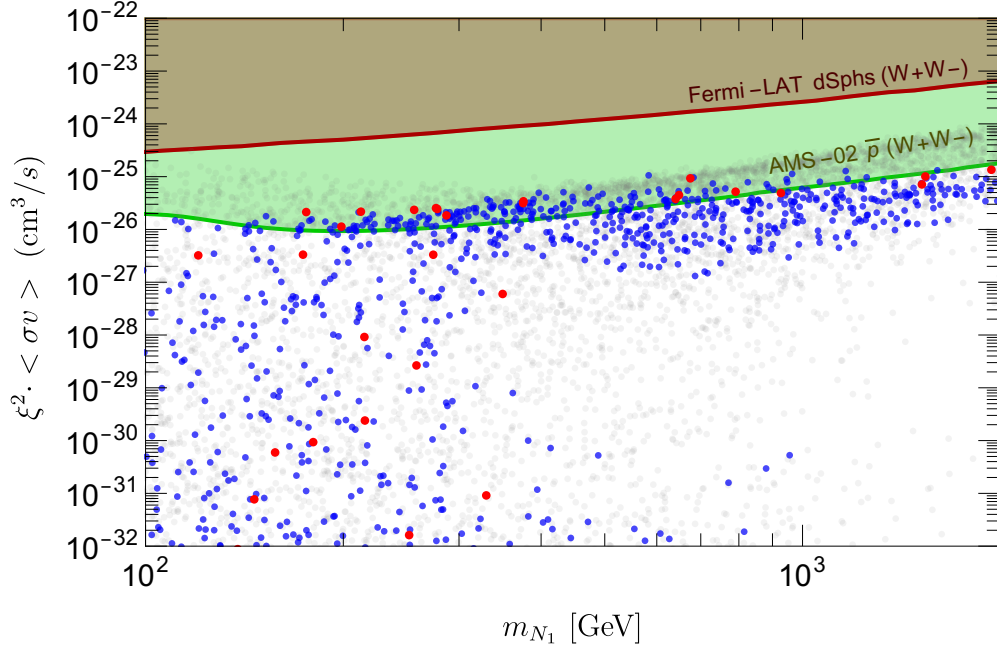


Figure 5: N_1 total annihilation cross section as a function of m_{N_1} . The red and green lines refer to the corresponding 95% C.L. upper limits currently set by Fermi-LAT gamma-ray data from dSphs [74] and from the antiproton and B/C data of AMS-02 [69], respectively.

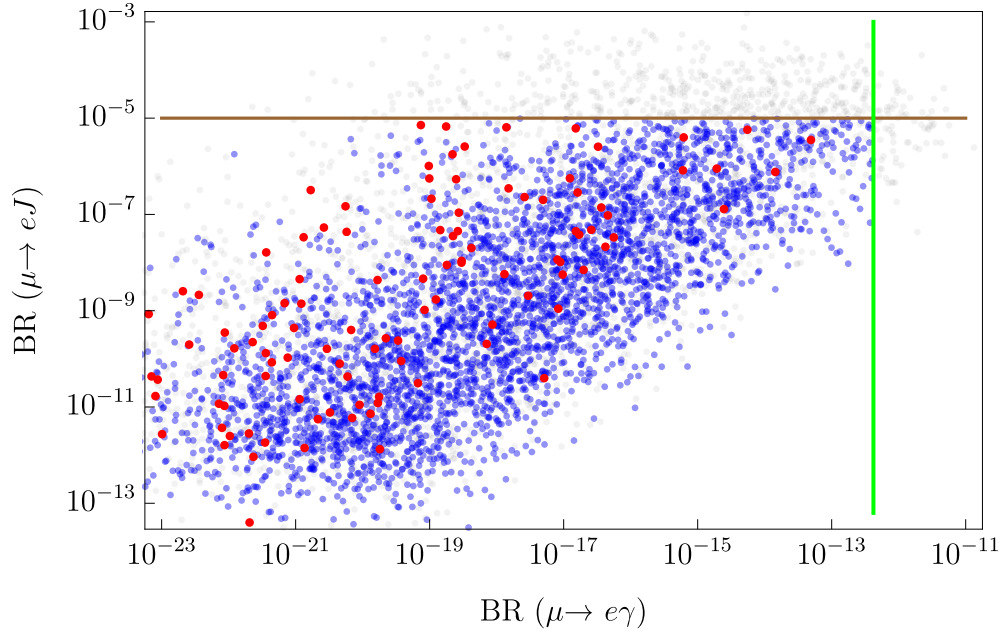


Figure 6: $\text{BR}(\mu \rightarrow eJ)$ as a function of $\text{BR}(\mu \rightarrow e\gamma)$ in the coannihilation region, where $\Delta \in [0, 20]$ GeV. Same color code as in Fig. 2. The horizontal and vertical lines correspond to the current experimental limits, discussed in Sec. 3.

5 Summary and discussion

Most SM extensions aiming at an explanation of neutrino oscillation data consider Majorana neutrinos. This option breaks the accidental $U(1)_L$ lepton number symmetry of the SM in two units. If the breaking of lepton number is spontaneous, a Goldstone boson appears in the particle spectrum of the theory, the majoron. In this work we have analyzed the dark matter phenomenology of this scenario in the context of the popular Scotogenic model.

Focusing on the fermionic DM candidate N_1 , we have found that it can explain the observed DM abundance in three regions of parameter space: (i) a resonant region where it annihilates via h_1 , with $m_{N_1} \sim 60$ GeV, (ii) a second resonant region where s -channel annihilations via h_2 are relevant and (iii) a region of coannihilations at $m_{N_1} \sim 1$ TeV. In particular, if coannihilations are relevant, more allowed solutions are found, either explaining the totality of DM or at least a sizeable part of it. While some of these solutions are already excluded by the recent LUX-ZEPLIN result, most of them are within the reach of near-future direct detection experiments. Interestingly, indirect detection searches seem to constitute another promising tool to further probe N_1 as a DM candidate via its multi-messenger signals, mainly gamma rays and antiprotons. All in all, the presence of the majoron and of a second Higgs open up the allowed parameter space of N_1 as DM, compared to the standard Scotogenic model. The majoron has an impact also on the phenomenology of LFV observables, as it leads to new interesting signatures, where it appears in the final state. Among these, we found that $\text{BR}(\mu \rightarrow eJ)$ is generally more constraining than the most common $\text{BR}(\mu \rightarrow e\gamma)$. Moreover, let us comment that the presence of a massless majoron may have relevant implications on the early-Universe cosmology. In particular, it can affect cosmological and astrophysical environments, and can contribute to ΔN_{eff} . In principle, these bounds could be relaxed if the majoron acquires a small mass (for instance from quantum gravity considerations). In such a case, the majoron would decay before Big Bang nucleosynthesis and would not affect cosmological observations. However, let us notice that, in order not to alter the phenomenological analysis presented in this paper, the majoron mass should be smaller than the electron one and hence its only available decay channel would be into active neutrinos. On the other hand, the majoron can be produced from the Higgs decay, or the annihilation of N_1 or even via freeze-in through its small coupling with the active neutrinos. If it is massless and thermalizes, in order to avoid constraints from ΔN_{eff} , one should require the majoron to decouple before $T \sim 0.5$ GeV (see e.g. [75]) to avoid the current constraint from Planck. This can be easily obtained if $\lambda_3^{H\sigma}$ is set small enough ($\lesssim 10^{-5}$). In such a case, all majoron production channels through SM particles would be suppressed, and it could only be produced via interactions with N_1 , through the (sizeable) coupling κ . If this is the case, the majoron would freeze out at around the same time as N_1 , that is at $T_F \sim m_{N_1}/20$, thus not substantially contributing to ΔN_{eff} . We have checked that by imposing $\lambda_3^{H\sigma} \lesssim 10^{-5}$ our results remain almost unchanged, with the only exception of the second resonance shown in Fig. 2. This region would disappear, due to the fact that a tiny $\lambda_3^{H\sigma}$ suppresses all vertices involving a (heavy or light) Higgs.

Finally, another interesting scenario consists in N_1 having very tiny couplings, so that it does not reach thermal equilibrium in the early Universe and it is instead produced via freeze-in. Such a production mechanism, yet together with the presence of the majoron, should also lead to some interesting phenomenology. We leave such analysis for a follow-up

of this paper.

Acknowledgements

The authors are grateful to Víctor Martín-Lozano for enlightening discussions on collider constraints in our scenario. Work supported by the Spanish grants PID2020-113775GB-I00 (AEI/10.13039/501100011033), CIPROM/2021/054, SEJI/2018/033 and SEJI/2020/016 (Generalitat Valenciana). AV acknowledges financial support from MINECO through the Ramón y Cajal contract RYC2018-025795-I. VDR acknowledges financial support by the Universitat de València through the sub-programme “ATRACCIÓ DE TALENT 2019”, in the early stages of this work.

References

- [1] P. F. de Salas, D. V. Forero, S. Gariazzo, P. Martínez-Miravé, O. Mena, C. A. Ternes, M. Tórtola, and J. W. F. Valle, “2020 global reassessment of the neutrino oscillation picture,” *JHEP* **02** (2021) 071, [arXiv:2006.11237 \[hep-ph\]](#).
- [2] **Planck** Collaboration, N. Aghanim *et al.*, “Planck 2018 results. VI. Cosmological parameters,” *Astron. Astrophys.* **641** (2020) A6, [arXiv:1807.06209 \[astro-ph.CO\]](#). [Erratum: *Astron. Astrophys.* 652, C4 (2021)].
- [3] A. Zee, “A Theory of Lepton Number Violation, Neutrino Majorana Mass, and Oscillation,” *Phys. Lett. B* **93** (1980) 389. [Erratum: *Phys. Lett. B* 95, 461 (1980)].
- [4] T. P. Cheng and L.-F. Li, “Neutrino Masses, Mixings and Oscillations in $SU(2) \times U(1)$ Models of Electroweak Interactions,” *Phys. Rev. D* **22** (1980) 2860.
- [5] A. Zee, “Quantum Numbers of Majorana Neutrino Masses,” *Nucl. Phys. B* **264** (1986) 99–110.
- [6] K. S. Babu, “Model of ‘Calculable’ Majorana Neutrino Masses,” *Phys. Lett. B* **203** (1988) 132–136.
- [7] Y. Cai, J. Herrero-García, M. A. Schmidt, A. Vicente, and R. R. Volkas, “From the trees to the forest: a review of radiative neutrino mass models,” *Front. in Phys.* **5** (2017) 63, [arXiv:1706.08524 \[hep-ph\]](#).
- [8] E. Ma, “Verifiable radiative seesaw mechanism of neutrino mass and dark matter,” *Phys. Rev. D* **73** (2006) 077301, [arXiv:hep-ph/0601225](#).
- [9] Y. Chikashige, R. N. Mohapatra, and R. D. Peccei, “Spontaneously Broken Lepton Number and Cosmological Constraints on the Neutrino Mass Spectrum,” *Phys. Rev. Lett.* **45** (1980) 1926.
- [10] Y. Chikashige, R. N. Mohapatra, and R. D. Peccei, “Are There Real Goldstone Bosons Associated with Broken Lepton Number?,” *Phys. Lett. B* **98** (1981) 265–268.

- [11] G. B. Gelmini and M. Roncadelli, “Left-Handed Neutrino Mass Scale and Spontaneously Broken Lepton Number,” *Phys. Lett. B* **99** (1981) 411–415.
- [12] J. Schechter and J. W. F. Valle, “Neutrino Decay and Spontaneous Violation of Lepton Number,” *Phys. Rev. D* **25** (1982) 774.
- [13] C. S. Aulakh and R. N. Mohapatra, “Neutrino as the Supersymmetric Partner of the Majoron,” *Phys. Lett. B* **119** (1982) 136–140.
- [14] C. Bonilla, L. M. G. de la Vega, J. M. Lamprea, R. A. Lineros, and E. Peinado, “Fermion Dark Matter and Radiative Neutrino Masses from Spontaneous Lepton Number Breaking,” *New J. Phys.* **22** no. 3, (2020) 033009, [arXiv:1908.04276 \[hep-ph\]](#).
- [15] P. Escribano and A. Vicente, “An ultraviolet completion for the Scotogenic model,” *Phys. Lett. B* **823** (2021) 136717, [arXiv:2107.10265 \[hep-ph\]](#).
- [16] E. Ma and V. De Romeri, “Radiative seesaw dark matter,” *Phys. Rev. D* **104** no. 5, (2021) 055004, [arXiv:2105.00552 \[hep-ph\]](#).
- [17] K. S. Babu and E. Ma, “Singlet fermion dark matter and electroweak baryogenesis with radiative neutrino mass,” *Int. J. Mod. Phys. A* **23** (2008) 1813–1819, [arXiv:0708.3790 \[hep-ph\]](#).
- [18] S. Mandal, N. Rojas, R. Srivastava, and J. W. F. Valle, “Dark matter as the origin of neutrino mass in the inverse seesaw mechanism,” *Phys. Lett. B* **821** (2021) 136609, [arXiv:1907.07728 \[hep-ph\]](#).
- [19] D. W. Kang, J. Kim, and H. Okada, “Muon $g - 2$ in $U(1)_{\mu-\tau}$ symmetric gauged radiative neutrino mass model,” *Phys. Lett. B* **822** (2021) 136666, [arXiv:2107.09960 \[hep-ph\]](#).
- [20] G. ’t Hooft, “Naturalness, chiral symmetry, and spontaneous chiral symmetry breaking,” *NATO Sci. Ser. B* **59** (1980) 135–157.
- [21] M. Kadastik, K. Kannike, and M. Raidal, “Dark Matter as the signal of Grand Unification,” *Phys. Rev. D* **80** (2009) 085020, [arXiv:0907.1894 \[hep-ph\]](#). [Erratum: *Phys.Rev.D* **81**, 029903 (2010)].
- [22] CMS Collaboration, A. M. Sirunyan *et al.*, “Search for invisible decays of a Higgs boson produced through vector boson fusion in proton-proton collisions at $\sqrt{s} = 13$ TeV,” *Phys. Lett. B* **793** (2019) 520–551, [arXiv:1809.05937 \[hep-ex\]](#).
- [23] T. Biekötter and M. Pierre, “Higgs-boson visible and invisible constraints on hidden sectors,” [arXiv:2208.05505 \[hep-ph\]](#).
- [24] M. E. Peskin and T. Takeuchi, “Estimation of oblique electroweak corrections,” *Phys. Rev. D* **46** (1992) 381–409.

- [25] **Particle Data Group** Collaboration, P. A. Zyla *et al.*, “Review of Particle Physics,” *PTEP* **2020** no. 8, (2020) 083C01.
- [26] J. A. Casas and A. Ibarra, “Oscillating neutrinos and $\mu \rightarrow e, \gamma$,” *Nucl. Phys. B* **618** (2001) 171–204, [arXiv:hep-ph/0103065](#).
- [27] T. Toma and A. Vicente, “Lepton Flavor Violation in the Scotogenic Model,” *JHEP* **01** (2014) 160, [arXiv:1312.2840 \[hep-ph\]](#).
- [28] I. Cordero-Carrión, M. Hirsch, and A. Vicente, “Master Majorana neutrino mass parametrization,” *Phys. Rev. D* **99** no. 7, (2019) 075019, [arXiv:1812.03896 \[hep-ph\]](#).
- [29] I. Cordero-Carrión, M. Hirsch, and A. Vicente, “General parametrization of Majorana neutrino mass models,” *Phys. Rev. D* **101** no. 7, (2020) 075032, [arXiv:1912.08858 \[hep-ph\]](#).
- [30] P. Escribano and A. Vicente, “Ultralight scalars in leptonic observables,” *JHEP* **03** (2021) 240, [arXiv:2008.01099 \[hep-ph\]](#).
- [31] G. Raffelt and A. Weiss, “Red giant bound on the axion - electron coupling revisited,” *Phys. Rev. D* **51** (1995) 1495–1498, [arXiv:hep-ph/9410205](#).
- [32] L. Di Luzio, M. Giannotti, E. Nardi, and L. Visinelli, “The landscape of QCD axion models,” *Phys. Rept.* **870** (2020) 1–117, [arXiv:2003.01100 \[hep-ph\]](#).
- [33] L. Calibbi, D. Redigolo, R. Ziegler, and J. Zupan, “Looking forward to lepton-flavor-violating ALPs,” *JHEP* **09** (2021) 173, [arXiv:2006.04795 \[hep-ph\]](#).
- [34] R. Bollig, W. DeRocco, P. W. Graham, and H.-T. Janka, “Muons in Supernovae: Implications for the Axion-Muon Coupling,” *Phys. Rev. Lett.* **125** no. 5, (2020) 051104, [arXiv:2005.07141 \[hep-ph\]](#). [Erratum: *Phys.Rev.Lett.* 126, 189901 (2021)].
- [35] D. Croon, G. Elor, R. K. Leane, and S. D. McDermott, “Supernova Muons: New Constraints on Z' Bosons, Axions and ALPs,” *JHEP* **01** (2021) 107, [arXiv:2006.13942 \[hep-ph\]](#).
- [36] R. Ballou *et al.*, “Latest Results of the OSQAR Photon Regeneration Experiment for Axion-Like Particle Search,” in *10th Patras Workshop on Axions, WIMPs and WISPs*, pp. 125–130. 2014. [arXiv:1410.2566 \[hep-ex\]](#).
- [37] **MEG** Collaboration, A. M. Baldini *et al.*, “Search for the lepton flavour violating decay $\mu^+ \rightarrow e^+ \gamma$ with the full dataset of the MEG experiment,” *Eur. Phys. J. C* **76** no. 8, (2016) 434, [arXiv:1605.05081 \[hep-ex\]](#).
- [38] A. Abada, M. E. Krauss, W. Porod, F. Staub, A. Vicente, and C. Weiland, “Lepton flavor violation in low-scale seesaw models: SUSY and non-SUSY contributions,” *JHEP* **11** (2014) 048, [arXiv:1408.0138 \[hep-ph\]](#).

- [39] A. Jodidio *et al.*, “Search for Right-Handed Currents in Muon Decay,” *Phys. Rev. D* **34** (1986) 1967. [Erratum: *Phys.Rev.D* 37, 237 (1988)].
- [40] M. Hirsch, A. Vicente, J. Meyer, and W. Porod, “Majoron emission in muon and tau decays revisited,” *Phys. Rev. D* **79** (2009) 055023, [arXiv:0902.0525 \[hep-ph\]](#). [Erratum: *Phys.Rev.D* 79, 079901 (2009)].
- [41] Y. Farzan, “Bounds on the coupling of the Majoron to light neutrinos from supernova cooling,” *Phys. Rev. D* **67** (2003) 073015, [arXiv:hep-ph/0211375](#).
- [42] F. Forastieri, M. Lattanzi, and P. Natoli, “Constraints on secret neutrino interactions after Planck,” *JCAP* **07** (2015) 014, [arXiv:1504.04999 \[astro-ph.CO\]](#).
- [43] Z. G. Berezhiani, A. Y. Smirnov, and J. W. F. Valle, “Observable Majoron emission in neutrinoless double beta decay,” *Phys. Lett. B* **291** (1992) 99–105, [arXiv:hep-ph/9207209](#).
- [44] A. P. Lessa and O. L. G. Peres, “Revising limits on neutrino-Majoron couplings,” *Phys. Rev. D* **75** (2007) 094001, [arXiv:hep-ph/0701068](#).
- [45] F. Staub, “SARAH 4 : A tool for (not only SUSY) model builders,” *Comput. Phys. Commun.* **185** (2014) 1773–1790, [arXiv:1309.7223 \[hep-ph\]](#).
- [46] A. Vicente, “Computer tools in particle physics,” [arXiv:1507.06349 \[hep-ph\]](#).
- [47] W. Porod, “SPheno, a program for calculating supersymmetric spectra, SUSY particle decays and SUSY particle production at e+ e- colliders,” *Comput. Phys. Commun.* **153** (2003) 275–315, [arXiv:hep-ph/0301101](#).
- [48] W. Porod and F. Staub, “SPheno 3.1: Extensions including flavour, CP-phases and models beyond the MSSM,” *Comput. Phys. Commun.* **183** (2012) 2458–2469, [arXiv:1104.1573 \[hep-ph\]](#).
- [49] W. Porod, F. Staub, and A. Vicente, “A Flavor Kit for BSM models,” *Eur. Phys. J. C* **74** no. 8, (2014) 2992, [arXiv:1405.1434 \[hep-ph\]](#).
- [50] G. Bélanger, F. Boudjema, A. Goudelis, A. Pukhov, and B. Zaldivar, “micrOMEGAs5.0 : Freeze-in,” *Comput. Phys. Commun.* **231** (2018) 173–186, [arXiv:1801.03509 \[hep-ph\]](#).
- [51] D. Aristizabal Sierra and C. E. Yaguna, “On the importance of the 1-loop finite corrections to seesaw neutrino masses,” *JHEP* **08** (2011) 013, [arXiv:1106.3587 \[hep-ph\]](#).
- [52] **LZ** Collaboration, J. Aalbers *et al.*, “First Dark Matter Search Results from the LUX-ZEPLIN (LZ) Experiment,” [arXiv:2207.03764 \[hep-ex\]](#).

- [53] **ATLAS** Collaboration, G. Aad *et al.*, “Searches for electroweak production of supersymmetric particles with compressed mass spectra in $\sqrt{s} = 13$ TeV pp collisions with the ATLAS detector,” *Phys. Rev. D* **101** no. 5, (2020) 052005, [arXiv:1911.12606 \[hep-ex\]](#).
- [54] **XENON** Collaboration, E. Aprile *et al.*, “Dark Matter Search Results from a One Ton-Year Exposure of XENON1T,” *Phys. Rev. Lett.* **121** no. 11, (2018) 111302, [arXiv:1805.12562 \[astro-ph.CO\]](#).
- [55] **PandaX-II** Collaboration, X. Cui *et al.*, “Dark Matter Results From 54-Ton-Day Exposure of PandaX-II Experiment,” *Phys. Rev. Lett.* **119** no. 18, (2017) 181302, [arXiv:1708.06917 \[astro-ph.CO\]](#).
- [56] **DarkSide** Collaboration, P. Agnes *et al.*, “DarkSide-50 532-day Dark Matter Search with Low-Radioactivity Argon,” *Phys. Rev. D* **98** no. 10, (2018) 102006, [arXiv:1802.07198 \[astro-ph.CO\]](#).
- [57] **DEAP** Collaboration, R. Ajaj *et al.*, “Search for dark matter with a 231-day exposure of liquid argon using DEAP-3600 at SNOLAB,” *Phys. Rev. D* **100** no. 2, (2019) 022004, [arXiv:1902.04048 \[astro-ph.CO\]](#).
- [58] **XENON** Collaboration, E. Aprile *et al.*, “Projected WIMP sensitivity of the XENONnT dark matter experiment,” *JCAP* **11** (2020) 031, [arXiv:2007.08796 \[physics.ins-det\]](#).
- [59] **GADMC** Collaboration, C. Galbiati *et al.*, “Future Dark Matter Searches with Low-Radioactivity Argon,” *Input to the European Particle Physics Strategy Update 2018-2020* (2018) . https://indico.cern.ch/event/765096/contributions/3295671/attachments/1785196/2906164/DarkSide-Argo_ESPP_Dec_17_2017.pdf.
- [60] M. Schumann *et al.*, “Dark matter sensitivity of multi-ton liquid xenon detectors,” *JCAP* **1510** no. 10, (2015) 016, [arXiv:1506.08309 \[physics.ins-det\]](#).
- [61] **DARWIN** Collaboration, J. Aalbers *et al.*, “DARWIN: towards the ultimate dark matter detector,” *JCAP* **1611** (2016) 017, [arXiv:1606.07001 \[astro-ph.IM\]](#).
- [62] J. Billard *et al.*, “Direct Detection of Dark Matter – APPEC Committee Report,” [arXiv:2104.07634 \[hep-ex\]](#).
- [63] J. Billard, L. Strigari, and E. Figueroa-Feliciano, “Implication of neutrino backgrounds on the reach of next generation dark matter direct detection experiments,” *Phys. Rev. D* **89** no. 2, (2014) 023524, [arXiv:1307.5458 \[hep-ph\]](#).
- [64] D. Aristizabal Sierra, V. De Romeri, L. J. Flores, and D. K. Papoulias, “Impact of COHERENT measurements, cross section uncertainties and new interactions on the neutrino floor,” *JCAP* **01** no. 01, (2022) 055, [arXiv:2109.03247 \[hep-ph\]](#).
- [65] C. A. J. O’Hare, “New Definition of the Neutrino Floor for Direct Dark Matter Searches,” *Phys. Rev. Lett.* **127** no. 25, (2021) 251802, [arXiv:2109.03116 \[hep-ph\]](#).

- [66] D. S. Akerib *et al.*, “Snowmass2021 Cosmic Frontier Dark Matter Direct Detection to the Neutrino Fog,” in *2022 Snowmass Summer Study*. 3, 2022. [arXiv:2203.08084 \[hep-ex\]](#).
- [67] M. Cirelli, G. Corcella, A. Hektor, G. Hutsi, M. Kadastik, P. Panci, M. Raidal, F. Sala, and A. Strumia, “PPPC 4 DM ID: A Poor Particle Physicist Cookbook for Dark Matter Indirect Detection,” *JCAP* **03** (2011) 051, [arXiv:1012.4515 \[hep-ph\]](#). [Erratum: JCAP 10, E01 (2012)].
- [68] **AMS** Collaboration, M. Aguilar *et al.*, “Antiproton Flux, Antiproton-to-Proton Flux Ratio, and Properties of Elementary Particle Fluxes in Primary Cosmic Rays Measured with the Alpha Magnetic Spectrometer on the International Space Station,” *Phys. Rev. Lett.* **117** no. 9, (2016) 091103.
- [69] A. Reinert and M. W. Winkler, “A Precision Search for WIMPs with Charged Cosmic Rays,” *JCAP* **01** (2018) 055, [arXiv:1712.00002 \[astro-ph.HE\]](#).
- [70] A. Cuoco, J. Heisig, M. Korsmeier, and M. Krämer, “Constraining heavy dark matter with cosmic-ray antiprotons,” *JCAP* **04** (2018) 004, [arXiv:1711.05274 \[hep-ph\]](#).
- [71] A. Cuoco, J. Heisig, L. Klamt, M. Korsmeier, and M. Krämer, “Scrutinizing the evidence for dark matter in cosmic-ray antiprotons,” *Phys. Rev. D* **99** no. 10, (2019) 103014, [arXiv:1903.01472 \[astro-ph.HE\]](#).
- [72] I. Cholis, T. Linden, and D. Hooper, “A Robust Excess in the Cosmic-Ray Antiproton Spectrum: Implications for Annihilating Dark Matter,” *Phys. Rev. D* **99** no. 10, (2019) 103026, [arXiv:1903.02549 \[astro-ph.HE\]](#).
- [73] J. Heisig, M. Korsmeier, and M. W. Winkler, “Dark matter or correlated errors: Systematics of the AMS-02 antiproton excess,” *Phys. Rev. Res.* **2** no. 4, (2020) 043017, [arXiv:2005.04237 \[astro-ph.HE\]](#).
- [74] **Fermi-LAT** Collaboration, M. Ackermann *et al.*, “Searching for Dark Matter Annihilation from Milky Way Dwarf Spheroidal Galaxies with Six Years of Fermi Large Area Telescope Data,” *Phys. Rev. Lett.* **115** no. 23, (2015) 231301, [arXiv:1503.02641 \[astro-ph.HE\]](#).
- [75] D. Baumann, D. Green, and B. Wallisch, “New Target for Cosmic Axion Searches,” *Phys. Rev. Lett.* **117** no. 17, (2016) 171301, [arXiv:1604.08614 \[astro-ph.CO\]](#).